Piezocatalysis

DOI: 10.1002/anie.201201424

Piezopotential-Driven Redox Reactions at the Surface of Piezoelectric Materials**

*Matthew B. Starr, Jian Shi, and Xudong Wang**

The manipulation of charge-carrier conduction characteristics is a critical attribute governing the operation and efficiency of photovoltaic, catalytic, and other energy-converting systems that are based on electrochemical principles.[1–9] This manipulation is often accomplished through the application of electrical-potential gradients by an external power supply and/or the creation of electronic-state discontinuities by heterojunction-interface engineering.[10–14] For example, in electrochemical systems, the transport of charge across chemical phases is governed by the energy and density of electronic states within the disparate phases as well as any existing bias between said phases.[15,16]

Piezoelectric materials have long been used as a source of bias and mechanical displacement, relying on their mechanical to electrical coupling character for applications in sensors,[17] actuators,[18] and energy harvesters.[19–22] In contrast to this historical precedent, contemporary integration of piezoelectric materials in semiconductor heterostructures capitalizes on the capability of the piezoelectric potential to manipulate charge carriers (i.e., piezotronics).[23–27] For instance, the straining of a piezoelectric element in order to change its semiconducting properties has recently been investigated in zinc oxide nanomaterials,[28,29] which have opened the doors to strain-gated logic operations and new possibilities for microelectronic circuitry elements. Straining effects in piezoelectric photoelectrochemical cells have also been shown to result in performance enhancements through manipulation of interface energetics.[30]

In principle, the piezoelectric modulation of charge carrier energetics should extend beyond the bounds of the buried electronic interfaces explored to date, thus allowing the direct enhancement or suppression of electrochemical processes that occur at the interface of a piezoelectric material and a solution (i.e., piezocatalysis). Preliminary experiments have shown an evolution of H_2 and O_2 from mechanically agitated piezoelectric $BaTiO_3$ and ZnO microstructures in an aqueous sonication bath.[31] In order to elucidate the intriguing piezocatalytic phenomenon, we report a systematic study of the piezoelectric-potential-driven electrochemical H_2 evolution process that takes place at the electrodes located on the surface of the material. The results compliment the general trends expected from the combinatorial assemblage of piezoelectricity and electrochemistry. The H_2 evolution rates were dependent upon the oscillation frequency and amplitude of the piezoelectric material, in accordance with the combination of the direct piezoelectric effect and electrochemical reactions.

A study of the piezocatalytic effect was conducted on a single-crystalline ferroelectric $Pb(Mg_{1/3}Nb_{2/3})O_3$-32$PbTiO_3$ (PMN-PT) cantilever in a sealed chamber (see Figure S1 in the Supporting Information). The voltage output of the PMN-PT slab was first characterized in air (Figure 1a). The cantilever was mechanically oscillated with a fixed frequency and amplitude. When the piezoelectric cantilever was transitioned to the deionized water environment, the voltage amplitude decreased while the mechanical oscillation frequency and amplitude remained constant. In order to encompass the entire piezocatalytic system into a cohesive entity, an analogous circuit was constructed (Figure 1b). In this circuit, opposite and iteratively alternating sides of the piezoelectric material serve as both the working and counter electrodes, respectively. A strained piezoelectric material can be considered a charged capacitor, and thus the change in measured voltage is correlated with a change in piezoelectricity-induced surface charge (ΔQ_p). When a strained piezoelectric material is placed within an aqueous medium of finite conductivity and polarizability, its piezoelectricity-induced surface charge can be depleted through two primary pathways: Faradic (I_f) and capacitive ($I_c = dC_d V_d/dt$, in which C_d and V_d are the double layer capacitance and voltage drop across the double layer, respectively) currents:

$$\Delta Q_p = \int I_f \, dt + C_d V_d \quad (1)$$

The capacitive current leads to the formation of double layers in the vicinity of piezoelectric surfaces, thus screening the surface charge. The Faradic current involves charge transfer between the solution and piezoelectric surfaces, which is possible under bias and responsible for electrochemical reactions.

Figure 1c shows a means by which piezoelectric potential is sufficient to create a favorable energetics landscape for generating Faradic currents on opposite electrode surfaces,

[*] M. B. Starr, J. Shi, Dr. X. D. Wang
Department of Materials Science and Engineering
University of Wisconsin–Madison
1509 University Ave., Madison, WI 53706 (USA)
E-mail: xudong@engr.wisc.edu

[**] We thank Prof. H. Xu and Prof. E. Roden for granting access to hydrogen measurement equipment, and Prof. M. Anderson, Prof. B. Hammers, and Dr. Y. Hara for helpful discussions. We also thank TRS Technology Inc. and H.C. Materials Co. for providing PMN-PT samples, and the personnel of UW–Madison physics department machine shop for their assistance in manufacturing the apparatus. This work is supported by DARPA under grant No. N66001-11-1-4139, the National Science Foundation under grant No. DMR-0905914, and the UW–Madison graduate school.

Supporting information for this article is available on the WWW under http://dx.doi.org/10.1002/anie.201201424.

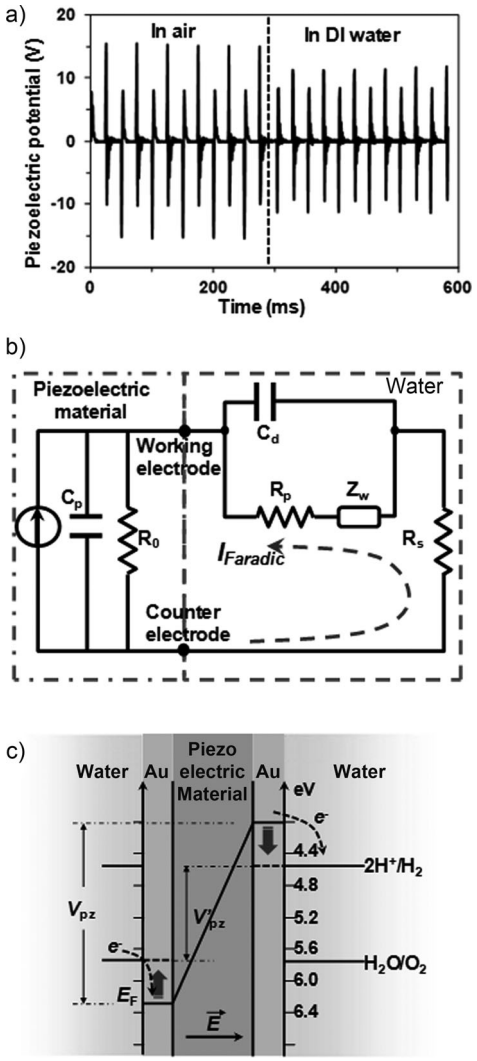

Figure 1. Fundamentals and preliminaries of piezocatalysis. a) Effect of environment on the measured piezoelectric potential. A marked decrease in potential difference is observed when the piezoelectric cantilever is moved from air to being submerged in deionized water. b) Proposed equivalence circuit based upon a first approximation combination of both a piezoelectric circuitry element and a charge-transfer/double layer analog for an electrochemical system. c) Proposed mechanism for the occurrence of piezoelectric-potential-driven Faradic currents at the piezoelectric/water interface.

thus promoting both the reduction of protons in solution (evolving H_2) and the oxidation of water. In the limit in which the piezoelectric material is a perfect dielectric, the appearance of piezoelectric potential induces a linear shift of the Fermi level. The electron energy levels of both electrodes follow the shift, and the difference is the observed piezoelectric voltage output (V_{pz}). Because neither of the electrodes is grounded, their absolute electrochemical potentials are considered "floating" and in intimate electrical contact with the pure water environment. Thus V_{pz} will shift the potential of both Au electrodes by an equal and opposite amount of $1/2\,eV_{pz}$ and $-1/2\,eV_{pz}$, respectively (solid lines in Au electrodes in Figure 1c). This electronic perturbation, which is induced by the mechanical deformation, modifies the energy level of electrons in the Au electrodes and moves it away from equilibrium. The difference in electrochemical potentials between the electrode and the solution are a driving force for electron transfer across the electrode/solution interface and thus induce electrochemical reactions. This process is similar to the one that occurs in an electrolysis system, in which an applied bias disrupts the equlibrium of the fermi level across the interface, thus resulting in a driving force for electrochemical reactions.

When the potential on the negative electrode exceeds the proton-reduction potential (right Au electrode in Figure 1c), electrons of sufficient energy could transfer from the electrode to protons on or near the surface, thus producing H_2. Similarly, when unoccupied electron energy levels of the electrode are made sufficiently positive in potential so as to exist below the water oxidation potential (left Au electrode in Figure 1c), electrons could transfer from water molecules to the electrode, thus producing O_2. Such piezoelectric-potential-driven electrochemical reactions create Faradic currents in the electrolyte and deplete piezoelectricity-induced surface charge. Therefore, the piezoelectric potential drops accordingly and eventually the reactions cease when the electron energy levels are no longer energetically favorable for net charge transfer (dashed lines in Au electrodes in Figure 1c). The Faradic capability of piezoelectric potential was experimentally demonstrated by characterizing the electrode potential relative to a saturated calomel electrode (SCE) through a potentiostat. Even with the solution resistance (R_S) of deionized water and with modest strain, the potential present on the electrode is sufficiently negative to thermodynamically engage the H_2 evolution reaction (Figure S2a–d in the Supporting Information).

Having verified that piezocatalyzed proton reduction is thermodynamically accessible, H_2 gas evolution was measured as a function of time, during mechanical oscillation of the piezoelectric cantilever in deionized water at given frequencies (Figure 2a). The strain amplitude was kept constant, generating a piezoelectric potential of 20 V throughout the entire experimental set. The triangles in Figure 2a represent H_2 concentrations in the reactor when the piezoelectric cantilever was oscillating at 10 Hz. Higher H_2 concentrations can be clearly observed at longer oscillation times. A linearized fit indicates the rate of H_2 concentration increase was approximately $0.22\ ppb\,s^{-1}$. By raising the oscillation rate to 20 Hz, the H_2 concentration was strikingly higher at given sampling times, though the data also exhibited a much wider distribution (solid diamonds in Figure 2a). The rate of increase of H_2 concentration suggested by the linearized fit was about $0.68\ ppb\,s^{-1}$. These H_2 production rates far exceeded (by at least one order of magnitude) that exhibited for the control, which consisted of a nonpiezoelectric (silicon) cantilever that was manufactured in an identical manner and mechanically oscillated at equal amplitude and frequency (circles in Figure 2a).

Figure 2b shows all the acquired data from both 10 Hz and 20 Hz oscillation rates normalized by the number of oscillation cycles. Although a wide distribution (from ≈ 0.01 to ≈ 0.08 ppb/oscillation) was obtained, the rate of H_2

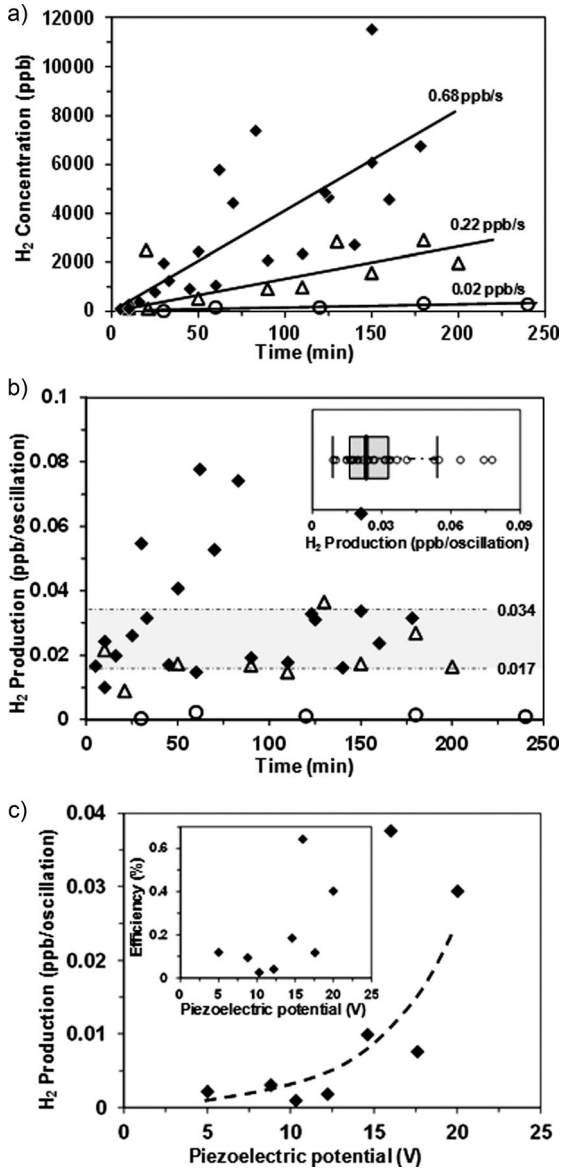

Figure 2. H_2 evolution correlated with the direct piezoelectric effect. a) H_2 concentrations measured as a function of oscillating time of the piezoelectric beam in deionized water with a frequency of 10 Hz (triangles) and 20 Hz (diamonds). A Si cantilever with identical configuration was used as a control (circles). b) H_2 production per oscillation derived from experiments shown in (a). Inset shows a box-whisker plot of the data given in (b) representing a reference for the dispersion. c) H_2 production per oscillation as a function of peak piezoelectric potential. An exponential dependence was identified (dashed line), consistent with the application of the Bulter–Volmer relationship. Inset shows the corresponding piezocatalytic efficiency calculated as a function of peak piezoelectric potential.

production remained within a constant range throughout an operation time that exceeded three hours (or $>220\,000$ cycles), thus indicating a stable H_2 evolution capability from the piezoelectric material. The H_2 production data were also analyzed by the Box–Whisker plot (inset of Figure 2b). The sample median has a value of approximately 0.024 ppb/oscillation. The upper and lower borders of the gray box represent the largest 25% and smallest 25% of the observations, thus corresponding to upper and lower limits of 0.034 and 0.017 ppb/oscillation, respectively. The data points outside the solid lines are classified as outliers.

H_2 output per oscillation was further investigated as a function of the piezoelectric potential. The H_2 production as a function of voltage is nonlinear and indeed follows an exponential relationship (Figure 2c). This observation is indicative of a case that is not limited by diffusion, likely because of the low current density (or H_2 production rate) and oscillation-self-induced agitation. The dependency of current density j on applied potential η is similar in form to that given by the Bulter–Volmer equation.[32]

$$j = j_0 e^{\frac{\alpha_c nF\eta}{RT}} \tag{2}$$

Fitting the data to such an exponential dependence gives an exchange current j_0 of 0.4 mA cm^{-2} and a cathodic transfer coefficient α_c of 0.002651. The small α_c possibly suggests that high overpotential would be necessary to drive the piezocatalytic process in the deionized water environment.[32] The agreement between the trend implied by theory and the experimental results is in accordance with basic principles. However, the time-dependent voltage–current relationship throughout an oscillation cycle would require a more complex, dynamic-j analysis to give the piezocatalysis mechanisms and kinetics with higher precision.

The electrical-to-chemical energy conversion efficiency (i.e., piezocatalytic efficiency) was estimated by comparing the total surface charge generated on the strained piezoelectric material to the amount of H_2 produced (inset of Figure 2c). The efficiency per oscillation is less than 0.7%, even under the favorable condition of high piezoelectric potential. Possible reasons for this inefficiency are: 1) voltage losses due to a capacitive current; and 2) an inability to carry out the electrochemical reaction to completion because of the insufficient time allotted for the piezoelectricity-induced surface charge to fully diminish through Faradic and/or capacitive currents.

If the time between one straining action to the next is less than the time necessary for the available energized surface charges to fully take part in the reaction, the ability of these charges to generate reaction products will be retarded. In order to demonstrate this influence toward the piezocatalytic efficiency, a new straining procedure was devised (Figure S3 in the Supporting Information). In this instance, the piezoelectric cantilever was put through a straining action in time t_1, held statically in the strained state for a time t_2, unstrained in a time $t_3 = t_1$, and held for a time $t_4 = t_2$. A typical voltage output by this manner of operation is shown in the inset of Figure 3a, where $t_1 = t_3 = 50$ ms, and $t_2 = t_4 = 2$ s. Holding the strain for an extended period of time (≈ 2 s) allowed the piezoelectricity-induced surface charge to fully deplete before the occurrence of an opposite strain and thus the revival of piezoelectric potential. The voltage-drop curve during one straining cycle is shown in Figure 3a. The majority (90%) of voltage decrease occurred within the first approximately 0.06 s, with 99% voltage drop having occurred by 1.46 s. To reveal the holding-time-dependent H_2 evolution, a series of experiments were conducted with various t_2 ($=t_4$) ranging

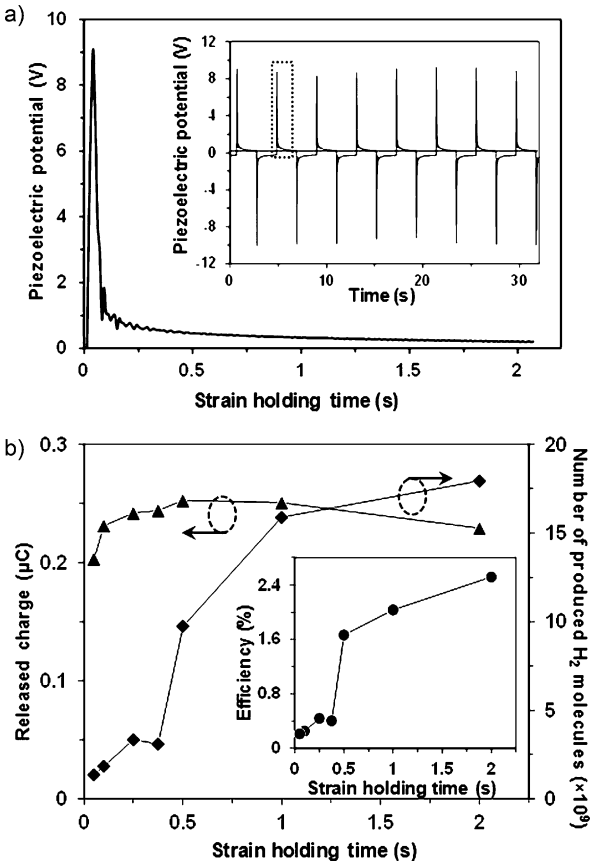

Figure 3. H_2 evolution correlated with the piezoelectric charge release. a) Piezoelectric potential curve obtained from the piezoelectric beam, when it was held under a constant strain in deionized water. Inset shows a typical piezoelectric potential profile with a strain holding time of two seconds. The dashed box shows the potential-decreasing cycle shown in (a). b) Total quantity of released charge (triangles) and corresponding number of produced H_2 molecules (diamonds) as functions of the strain holding time (peak piezoelectric potential was kept at $\approx$10 V). Inset shows the piezocatalytic efficiency of H_2 evolution per straining as a function of holding time.

from 0.05 to 2 s and a fixed $t_1 = t_3 = 50$ ms to ensure the same strain rate. From the output voltage profiles (Figure S4 in the Supporting Information), the quantity of charge that was depleted from each straining action was calculated (see Figure S5 in the Supporting Information for details) and plotted as a function of strain holding time (triangles in Figure 3b). The number of H_2 molecules produced during each straining cycle is also depicted on this plot as a function of holding time (diamonds). As a result of the rapid voltage drop, small variations of the released charge were observed at $t_2 > 0.2$ s; whereas the ability of the piezoelectric potential to drive the H_2 evolution reactions markedly improved as t_2 increased beyond 0.5 s, and approached its asymptote when $t_2 > \approx 1$ s. The discrepancy between the amounts of released charge and produced H_2 molecules at shorter t_2 indicates that the initial voltage drop may be mostly attributed to capacitive current, while Faradic charge transfer would occur in a steady but slow manner, and may only become dominating after the double layer has formed.

A comparison of the values of released charges to produced H_2 molecules gave the piezocatalytic efficiency per straining action as a function of t_2 (inset of Figure 3b). The efficiency results are consistent with those of reaction kinetics hindering the productivity of hasty oscillations, which clearly shows that the introduction of a holding period largely facilitated the H_2 generation. Given the same peak piezoelectric voltage ($\approx$10 V), a holding time of 50 ms improved the piezocatalytic efficiency from about 0.02% to more than 0.2%. With longer t_2 (1–2 s), the piezocatalytic efficiency reached approximately 2–2.4%. These values exceeded those of the 20 Hz oscillations by two orders of magnitude.

According to Equation (1), the double-layer capacitance (C_d) could also significantly impact the efficiency. Therefore, in piezocatalytic systems, a concentrated electrolyte might critically limit the effectiveness of the piezocatalytic process through an increase in C_d, and thus screening the piezoelectric potential, detrimentally sapping the free energy available for driving electrochemical reactions. In order to reveal the influences of electrolytes in piezocatalytic systems, piezocatalyzed H_2 evolution was conducted in $NaNO_3$ solution with concentrations varying from 1 μM to 1 mM. All the experiments were performed under the straining condition of $t_1 = t_3 = 50$ ms and $t_2 = t_4 = 1$ s. Figure 4a shows the peak piezoelectric voltages and corresponding H_2 production rates as functions of electrolyte concentration, together with the results from deionized water under the identical straining conditions.

The H_2 production rate dropped monotonically with the increase of electrolyte concentration. This clearly shows that

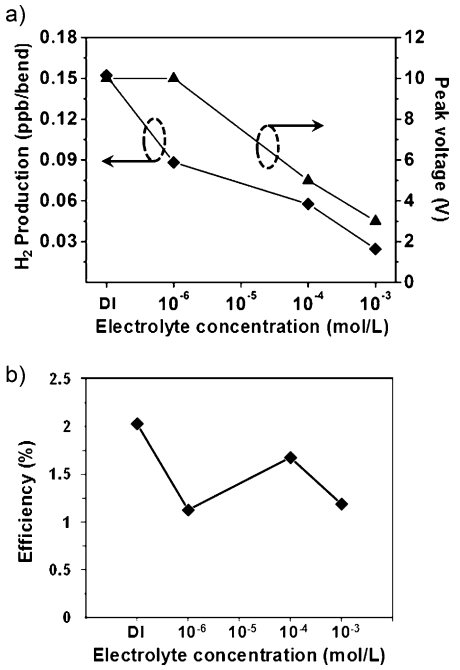

Figure 4. H_2 evolution correlated with electrolyte concentration. a) Peak piezoelectric voltage (triangles) and H_2 production rate (diamonds) as functions of electrolyte concentration. b) Corresponding piezocatalytic efficiency of H_2 production per strain as a function of electrolyte concentration.

the increased screening charge that results from a large C_d is capable to severely subdue the free-energy difference between the electrodes, and thus reduce the quantity of work possible in the form of electrochemical processes. This result is also manifest in the reduced maximum piezoelectric voltage at higher electrolyte concentrations, thus indicating a reduction in the number of surface charges. The calculated piezocatalytic efficiency therefore still exhibited comparable values ($\approx$1–2%, Figure 4b) as is the case in deionized water. These significantly high efficiencies, given the low piezoelectric voltages (3–5 V), are attributed to the improved R_s. Therefore, because of the finite amount of energized surface electrons and the charge-dictated potential amplitude, the piezocatalyzed H_2 evolution is heavily influenced by the magnitude of piezoelectric potential, the rate of charge exchange, and the formation of double layers.

In summary, a piezocatalysis system can directly exert energetic control over chemical species within its immediate vicinity, thus producing H_2 by straining a piezoelectric material in an aqueous solution. This discovery emboldens a new strategy for mechanically tailoring interface energetics and chemistry. Further exploration into how piezoelectric potentials can modulate the electronic states at the surface of the material may result in the facile enhancement of conventional catalyst materials while engaging catalytic processes in otherwise overlooked or discarded materials.

Experimental Section

A PMN-PT single crystal slab was used as the piezoelectric component for the piezoelectric cantilever. The PMN-PT slabs were poled along the $\langle 001 \rangle$ direction, and exhibit piezoelectric coefficients of 2200–2700 pCN^{-1}. Cantilever construction and encapsulation was accomplished with ECCOBOND® 45 epoxy. The entire assemblage was emerged in deionized water and $NaNO_3$ electrolytes within a sealed chamber with access ports for piezoelectric actuation and monitoring, environmental purging, and atmospheric sampling. Straining of the piezoelectric cantilever was achieved by a computer-controlled vibrator (for high-frequency oscillation) and linear actuator (for controlling straining state). The H_2 concentration was determined by measuring the atmosphere sample in the reactor using an AMETEK Analyzer ta3000F H_2 gas analyzer. A background baseline for atmospheric H_2 concentration was established before every experiment through a 10-minute nitrogen purging to the apparatus. The piezoelectric potential and the surface electrochemical potential were measured by a digital oscilloscope and a potentiostat, respectively.

Received: February 20, 2012
Revised: April 10, 2012
Published online: May 3, 2012

Keywords: electrochemistry · piezocatalysis · piezoelectricity · piezotronics · water splitting

[1] Y. B. Yuan, T. J. Reece, Y. P. Sharma, S. Poddar, S. Ducharme, A. Gruverman, Y. Yang, J. Huang, *Nat. Mater.* **2011**, *10*, 296–302.
[2] Y. D. Hou, B. L. Abrams, et al., *Nat. Mater.* **2011**, *10*, 434–438.
[3] X. Chen, L. Liu, P. Y. Yu, S. S. Mao, *Science* **2011**, *331*, 746–750.
[4] H. I. Karunadasa, C. J. Chang, J. R. Long, *Nature* **2010**, *464*, 1329–1333.
[5] M. R. Hoffmann, J. A. Moss, et al., *J. Chem. Soc. Dalton Trans.* **2011**, *40*, 5151–5158.
[6] X. B. Chen, S. H. Shen, L. J. Guo, S. S. Mao, *Chem. Rev.* **2010**, *110*, 6503–6570.
[7] J. Liu, G. Cao, Z. Yang, D. Wang, D. Dubois, X. Zhou, L. G. Graff, L. R. Pederson, J. Zhang, *ChemSusChem* **2008**, *1*, 676–697.
[8] E. Barton Cole, P. S. Lakkaraju, D. M. Rampulla, A. J. Morris, E. Abelev, A. B. Bocarsly, *J. Am. Chem. Soc.* **2010**, *132*, 11539–11551.
[9] J. Shi, Y. Hara, C. Sun, M. A. Anderson, X. Wang, *Nano Lett.* **2011**, *11*, 3413–3419.
[10] W. J. Yin, H. Tang, S. H. Wei, M. M. Al-Jassim, J. Turner, Y. Yan, *Phys. Rev. B* **2010**, *82*, 045106.
[11] B. R. Hyun, A. C. Bartnik, J. K. Lee, H.i Imoto, L. F. Sun, J. J. Choi, Y. Chujo, T. Hanrath, C. K. Ober, F. W. Wise, *Nano Lett.* **2011**, *11*, 2126–2132.
[12] C. L. Braun, *J. Chem. Phys.* **1984**, *80*, 4157–4161.
[13] S. L. Candelaria, Y. Shao, W. Zhou, X. Li, J. Xiao, J. Zhang, Y. Wang, J. Liu, J. Li, G. Cao, *Nano Energy* **2012**, *1*, 195–220.
[14] R. Hayoun, K. M. Whitaker, D. R. Gamelin, J. M. Maye, *J. Am. Chem. Soc.* **2011**, *133*, 4228–4231.
[15] N. S. Lewis, *Inorg. Chem.* **2005**, *44*, 6900–6911.
[16] A. J. Bard, L. R. Faulkner, *Electrochemical Methods: Fundamentals and Applications*, Wiley, New York, **2001**.
[17] J. F. Tressler, S. Alkoy, R. E. Newnham, *J. Electroceram.* **1998**, *2*, 257–272.
[18] D. J. Laser, J. G. Santiago, *J. Micromech. Microeng.* **2004**, *14*, R35–R64.
[19] X. D. Wang, J. H. Song, J. Liu, Z. L. Wang, *Science* **2007**, *316*, 102–105.
[20] Y. C. Shu, I. C. Lien, *Smart Mater. Struct.* **2006**, *15*, 1499–1512.
[21] S. Priya, *J. Electroceram.* **2007**, *19*, 167–184.
[22] A. Bhardwaj, N. V. Burbure, G. S. Rohrer, *J. Am. Ceram. Soc.* **2010**, *93*, 4129–4134.
[23] Z. L. Wang, *Nano Today* **2010**, *5*, 540–552.
[24] Y. Watanabe, *Phys. Rev. B* **1999**, *59*, 11257–11266.
[25] V. Garcia, M. Bibes, et al., *Science* **2010**, *327*, 1106–1110.
[26] D. Lee, S. H. Baek, T. H. Kim, J.-G. Yoon, C. M. Folkman, C. B. Eom, T. W. Noh, *Phys. Rev. B* **2011**, *84*, 125305.
[27] T. Choi, S. Lee, Y. J. Choi, V. Kiryukhin, S.-W. Cheong, *Science* **2009**, *324*, 63–66.
[28] W. Wu, Y. Wei, Z. L. Wang, *Adv. Mater.* **2010**, *22*, 4711–4715.
[29] W. Z. Wu, Z. L. Wang, *Nano Lett.* **2011**, *11*, 2779–2785.
[30] J. Shi, M. B. Starr, H. Xiang, Y. Hara, M. A. Anderson, J. H. Seo, Z. Ma, X. Wang, *Nano Lett.* **2011**, *11*, 5587–5593.
[31] K. S. Hong, H. Xu, H. Konishi, X. C. Li, *J. Phys. Chem. Lett.* **2010**, *1*, 997–1002.
[32] D. Pletcher, *A First Course in Electrode Processes*, Royal Society of Chemistry, Cambridge, **2009**.

